ISSN 1070-3284, Russian Journal of Coordination Chemistry, 2024, Vol. 50, No. 1, pp. 21–32. © Pleiades Publishing, Ltd., 2024.

Synthesis, Supramolecular Self-Organization, and Thermal Behavior of the Double Three-Dimensional Pseudo-Polymer Complex $[Au\{S_2CN(CH_2)_6\}_2]_4[Ag_5Cl_9]$ Comprising the New Type Silver(I) Anion

E. V. Korneeva[a], O. V. Loseva[a], A. I. Smolentsev[b], and A. V. Ivanov[a, *]

[a] *Institute of Geology and Nature Management, Far Eastern Branch, Russian Academy of Sciences, Blagoveshchensk, Russia*

[b] *Nikolaev Institute of Inorganic Chemistry, Siberian Branch, Novosibirsk, Russia*

**e-mail: alexander.v.ivanov@chemist.com*

Received March 10, 2023; revised April 6, 2023; accepted April 7, 2023

Abstract—New crystalline pseudo-polymer complex $[Au\{S_2CN(CH_2)_6\}_2]_4[Ag_5Cl_9]$ (**I**) was obtained by binding gold(III) with silver(I) hexamethylenedithiocarbamate from an $AuCl_3$/2.5 M NaCl solution. Complex **I** was isolated in a preparative yield and structurally characterized. The X-ray diffraction (XRD) data (CIF file CCDC no. 2205197) show that the isomeric cations of $[Au\{S_2CN(CH_2)_6\}_2]^+$ (A : 2B : C) and complicated pentanuclear anion $[Ag_5Cl_9]^{4-}$ are the main structural units of the compound. The supramolecular self-organization of the ionic structural units in complex **I** occurs due to multiple secondary interactions Cl···S and Ag···S, hydrogen bonds C–H···Cl, and anagostic interactions C–H···Ag, resulting in the formation of the 3D pseudo-polymer framework. The thermal behavior of complex **I** is studied by simultaneous thermal analysis to find that the thermolysis of the double Au(III)–Ag(I) compound is accompanied by the quantitative regeneration of the bound metals under comparatively mild conditions.

Keywords: double gold(III)–silver(I) complexes, pseudo-polymer compounds, supramolecular self-organization, secondary bonds (Ag···S, Cl···S), thermal behavior

DOI: 10.1134/S1070328423600572

INTRODUCTION

Dithiocarbamates (Dtc) and their derivatives find use in a number of practical fields: agriculture (pesticides and fungicides) [1, 2] and medicine. For example, tetraethyl thiuramdisulfide (trade mark Teturam or Disulfiram) has been used widely for several decades as an efficient therapeutic remedy for alcohol addiction. However, a high anticancer activity of this compound has been found rather recently [3, 4], which is additionally enhanced in a combination with Cu^{2+} ions (as it is believed, due to the formed copper(II) diethyldithiocarbamate [5, 6]). The studies of the silver(I) and gold(III) complexes comprising the dithiocarbamate ligands also made it possible to reveal their important, practically significant antibacterial, anticancer, and antitubercular activities [7–14].

In addition, we have earlier found for dialkyl(alkylene) dithiocarbamates of the number of transition metals, particularly, silver(I), the capability of efficient binding of gold(III) from solutions to the solid phase with the formation of double pseudo-polymer complexes, including the Au(III)–Ag(I) compounds [15–18]. Continuing these studies, we prepared the supramolecular complex: bis(*N*,*N*-*cyclo*-hexamethylenedithiocarbamato-*S*,*S*')gold(III) nonachloropentaargentate(I), $[Au\{S_2CN(CH_2)_6\}_2]_4[Ag_5Cl_9]$ (**I**), comprising a new pentanuclear silver(I) anion along with gold(III) cations. The synthesized compound was characterized in detail by IR spectroscopy, XRD, and simultaneous thermal analysis (STA).

EXPERIMENTAL

Gold(III) chloride was prepared as described previously [15] by the dissolution of metallic gold in aqua regia followed by the evaporation of the solution. Sodium hexamethylenedithiocarbamate (HmDtc) was synthesized by the reaction of carbon sulfide (Merck) with hexamethyleneimine (Aldrich) in an alkaline medium [19]. Silver(I) hexamethylenedithiocarbamate [Ag(S_2CNHm)] was precipitated by the interaction of aqueous solutions of $AgNO_3$ and $Na\{S_2CN(CH_2)_6\}\cdot 2H_2O$. To prepare the silver(I) complex (100 mg), a solution of $AgNO_3$ (0.060 g, 0.354 mmol) in water (50 mL) was poured with stirring to a solution of $Na(S_2CNHm)\cdot 2H_2O$ (0.087 g, 0.370 mmol) in water (50 mL). The prepared precipi-

tate of [Ag(S_2CNHm)] was separated by filtration and washed on the filter. The IR spectroscopy data for the initial sodium salt and silver(I) complex coincide with the previously published spectral characteristics for these compounds [20, 21].

Synthesis of [Au{$S_2CN(CH_2)_6$}$_2$]$_4$[Ag_5Cl_9] (I) was carried out by the reaction of freshly precipitated silver(I) hexamethylenedithiocarbamate with an $AuCl_3$/2.5 M NaCl solution: 10 mL of a solution of Na[$AuCl_4$] containing gold(III) (35.0 mg, 0.178 mmol) were poured to [Ag(S_2CNHm)] (100 mg, 0.354 mmol), and the resulting mixture was stirred at room temperature for 1 h. The degree of binding of gold from the solution to the solid phase was 99.27% indicating the formation of new compounds in the studied system. (The residual gold content in the solution after extraction was determined on a Hitachi (1 class, model 180–50) atomic absorption spectrometer). The formed yellow-orange precipitate was filtered off, washed with water, and dried on the filter. The precipitate is characterized by the partial dissolution in acetone, and transparent yellow prismatic crystals were grown for an XRD experiment from the resulting solution by the slow evaporation of the solvent at room temperature. The yield was 29.1%. (The remained portion of the precipitate was dissolved in chloroform, and crystals of the [Au(S_2CNHm)$_2$]$_2$[$AgCl_2$]Cl complex we characterized previously [18] were obtained from the solution.) The formation of complex **I** can be presented as follows:

$$8[Ag(S_2CNHm)] + 4Na[AuCl_4] = [Au(S_2CNHm)_2]_4[Ag_5Cl_9] + 3Na[AgCl_2] + NaCl.$$

For $C_{56}H_{96}N_8S_{16}Cl_9Ag_5Au_4$

Anal. calcd., %	C, 22.12	H, 3.18	N, 3.68	S, 16.87
Found, %	C, 22.48	H, 3.25	N, 3.79	S, 16.63

IR (ATR; ν, cm^{-1}): 2916, 2848, 1533, 1467, 1435, 1357, 1342, 1271, 1202, 1164, 1092, 1006, 994, 976, 960, 905, 878, 849, 824, 752, 621, 559, 506, 474, 464, 446, 430.

Elemental analysis was carried out on a Carlo Erba EA 1108 C,H,N,S automated analyzer. IR spectra were recorded on a Perkin-Elmer Spectrum 65 FT-IR spectrophotometer by the attenuated total internal reflectance (ATR) method in a frequency range of 400–4000 cm^{-1}. A JSM 6390LV JEOL scanning electron microscope (Japan) equipped with an INCAPentaFETx3 analytical system of X-ray spectral microanalysis with energy dispersion (Oxford Instrument, Great Britain) was used to determine dispersity, morphological features, and qualitative elemental composition of the studied substances.

XRD of single crystals of complex **I** was carried out on a Bruker-Nonius X8 Apex diffractometer (CCD detector, MoK_α, λ = 0.71073 Å, graphite monochromator) at 296(2) K. Data were collected using the standard procedure: φ and ω scan modes of narrow frames. An absorption correction was applied empirically using the SADABS program [22]. The structure was determined by a direct method and refined by least squares (for F^2) in the full-matrix anisotropic approximation of non-hydrogen atoms. Positions of hydrogen atoms in the HmDtc ligands were calculated geometrically and refined using a riding model. The calculations and structure refinement of compound **I** were performed using the SHELXL 2018/3 program [23]. The main crystallographic data and structure refinement parameters are given in Table 1. Selected bond lengths and angles are listed in Table 2. The geometric parameters of the hydrogen and chalcogen bonds, C–H···Cl and C–S···Cl, and anagostic interactions C–H···Ag are given in Table 3.

The coordinates of atoms, bond lengths, and angles were deposited with the Cambridge Crystallographic Data Centre (CIF file CCDC no. 2205197; deposit@ccdc.cam.ac.uk or http://www.ccdc.cam.ac.uk).

The thermal behavior of compound **I** was studied by STA for parallel detection of the thermogravimetry (TG) and differential scanning calorimetry (DSC) curves. The study was conducted on an STA 449C Jupiter instrument (NETZSCH) in corundum crucibles under caps with a hole providing a vapor pressure of 1 atm for the thermal decomposition of the sample. The heating rate was 5°C/min below 1100°C in an argon atmosphere. The sample mass was 2.095–7.840 mg. The accuracy of temperature measurement was ±0.9°C, and that for the mass change was $\pm 1 \times 10^{-4}$ mg. The correction file and the temperature and sensitivity calibrations for the specified temperature program and heating rate were used when recording the TG and DSC curves. The independent determination of the melting point was conducted on a PTP(M) instrument (OJSC Khimlaborpribor, Russia).

RESULTS AND DISCUSSION

Freshly precipitated silver(I) hexamethylenedithiocarbamate is a voluminous yellow-green precipitate,[1] whose energy dispersive spectrum exhibits characteristic peaks of Ag, S, and N (Fig. 1a). The interaction of the precipitate of the silver(I) complex with a bright yellow solution of Na[$AuCl_4$] results in the fast change in its color from yellow-green to red-orange already within the first minutes, and then the transition to a more saturated orange color is observed with

[1] The solvated form of the hexanuclear silver(I) cluster [Ag_6(HmDtc)$_6$]·$2CH_2Cl_2$ was earlier prepared by the recrystallization of the complex from a dichloromethane solution and structurally characterized [20].

Table 1. Crystallographic data and experimental and structure refinement parameters for compound **I**

Parameter	Value
Empirical formula	$C_{56}H_{96}N_8S_{16}Cl_9Ag_5Au_4$
FW	3040.63
Crystal system	Triclinic
Space group	$P\bar{1}$
a, Å	12.6761(3)
b, Å	12.7445(4)
c, Å	15.8773(4)
α, deg	72.7100(10)
β, deg	70.7640(10)
γ, deg	72.2460(10)
V, Å^3	2250.56(11)
Z	1
ρ_{calc}, g/cm^3	2.243
$\mu(MoK_\alpha)$, cm^{-1}	8.232
F(000)	1448
Crystal size, mm^3	0.24 × 0.14 × 0.10
Range of data collection for θ, deg	1.392–27.552
Ranges of reflection indices	$-16 \le h \le 15$, $-16 \le k \le 16$, $-20 \le l \le 14$
Measured reflections	25179
Independent reflections (R_{int})	10366 (0.0460)
Reflections with $I > 2\sigma(I)$	7073
Refinement variables	454
GOOF	1.041
R_1, wR_2 ($F^2 > 2\sigma(F^2)$)	0.0482, 0.1137
R_1, wR_2 (all reflections)	0.0809, 0.1238
Residual electron density (min/max), e/Å^3	−2.324/1.877

the simultaneous bleaching of the solution. The observed changes directly indicate the binding of gold(III) from the solution to the solid phase with the formation of a new compound, which is confirmed by the data of energy dispersive X-ray spectroscopy: the corresponding spectrum of the prepared orange powder expectedly contains the characteristic peaks of Au and Cl along with those of Ag and S (Fig. 1b). In addition, the scanning electron microscopy data show that the gold(III) binding is accompanied by the transformation of the precipitate of the initial complex with a change in the particle size and shape (Fig. 1).

The characteristic absorption bands caused by stretching vibrations of nearly all types of groups and bonds in the HmDtc ligands were identified in the IR spectrum of complex **I**. For example, the intense group at 1533 cm^{-1} corresponds to vibrations of the N–C bonds in the dithiocarbamate groups. Since the discussed band is appreciably shifted to the high-frequency range (which is characteristic of the double gold–silver dithiocarbamate chloride complexes [15, 16, 18]) compared to the initial silver(I) complex (1494 cm^{-1} [20]) and sodium salt $Na(S_2CNHm)\cdot 2H_2O$ (1485 cm^{-1} [21]), it can be concluded that the contribution of double bonding to the formally ordinary N–C(S)S bonds in compound **I** increases. In addition, the –NC(S)S– groups are also characterized by the absorption bands that reflect

Table 2. Selected bond lengths (*d*) and bond (ω) and torsion (φ) angles in the structure of compound **I***

Bond	*d*, Å	Bond	*d*, Å
Cation *A*			
Au(1)–S(11)	2.334(2)	N(1)–C(7)	1.469(9)
Au(1)–S(12)	2.346(2)	C(2)–C(3)	1.497(12)
S(11)–C(1)	1.715(8)	C(3)–C(4)	1.516(12)
S(12)–C(1)	1.756(8)	C(4)–C(5)	1.520(11)
N(1)–C(1)	1.288(10)	C(5)–C(6)	1.513(8)
N(1)–C(2)	1.488(10)	C(6)–C(7)	1.512(11)
Cation *B*			
Au(2)–S(21)	2.337(2)	N(3)–C(16)	1.448(9)
Au(2)–S(22)	2.327(2)	N(3)–C(21)	1.477(10)
Au(2)–S(23)	2.332(2)	C(9)–C(10)	1.518(8)
Au(2)–S(24)	2.336(2)	C(10)–C(11)	1.509(8)
S(21)–C(8)	1.733(7)	C(11)–C(12)	1.506(8)
S(22)–C(8)	1.721(8)	C(12)–C(13)	1.516(14)
S(23)–C(15)	1.721(8)	C(13)–C(14)	1.525(12)
S(24)–C(15)	1.727(7)	C(16)–C(17)	1.539(12)
N(2)–C(8)	1.316(9)	C(17)–C(18)	1.503(13)
N(2)–C(9)	1.473(10)	C(18)–C(19)	1.545(13)
N(2)–C(14)	1.451(9)	C(19)–C(20)	1.511(14)
N(3)–C(15)	1.310(9)	C(20)–C(21)	1.511(8)
Cation *C*			
Au(3)–S(31)	2.338(3)	N(4)–C(28)	1.468(12)
Au(3)–S(32)	2.332(3)	C(23)–C(24)	1.549(9)
S(31)–C(22)	1.734(10)	C(24)–C(25)	1.523(8)
S(32)–C(22)	1.746(10)	C(25)–C(26)	1.506(8)
N(4)–C(22)	1.280(12)	C(26)–C(27)	1.511(9)
N(4)–C(23)	1.460(13)	C(27)–C(28)	1.507(9)
Angle	ω, deg	Angle	ω, deg
Cation *A*			
S(11)Au(1)S(12)	75.55(7)	Au(1)S(12)C(1)	85.9(3)
S(11)Au(1)S(12)[a]	104.45(7)	S(11)C(1)S(12)	111.4(5)
Au(1)S(11)C(1)	87.2(3)		
Cation *B*			
S(21)Au(2)S(22)	75.57(7)	Au(2)S(21)C(8)	86.1(3)
S(21)Au(2)S(23)	105.68(7)	Au(2)S(22)C(8)	86.7(2)
S(21)Au(2)S(24)	175.96(8)	Au(2)S(23)C(15)	86.6(2)
S(22)Au(2)S(23)	178.47(8)	Au(2)S(24)C(15)	86.4(3)
S(22)Au(2)S(24)	103.59(8)	S(21)C(8)S(22)	111.7(4)
S(23)Au(2)S(24)	75.23(7)	S(23)C(15)S(24)	111.5(4)
Cation *C*			
S(31)Au(3)S(32)	75.28(9)	Au(3)S(32)C(22)	87.2(3)
S(31)Au(3)S(32)[b]	104.72(9)	S(31)C(22)S(32)	110.0(6)
Au(3)S(31)C(22)	87.3(4)		

Table 2. (Contd.)

Angle	φ, deg	Angle	φ, deg
Cation *A*			
Au(1)S(11)S(12)C(1)	−179.5(5)	S(11)C(1)N(1)C(7)	177.9(6)
S(11)Au(1)C(1)S(12)	−179.5(4)	S(12)C(1)N(1)C(2)	172.7(6)
S(11)C(1)N(1)C(2)	−6.7(11)	S(12)C(1)N(1)C(7)	−2.8(11)
Cation *B*			
Au(2)S(21)S(22)C(8)	−178.2(5)	S(22)C(8)N(2)C(9)	178.2(6)
Au(2)S(23)S(24)C(15)	174.1(5)	S(22)C(8)N(2)C(14)	−1.6(11)
S(21)Au(2)C(8)S(22)	−178.4(4)	S(23)C(15)N(3)C(16)	1.9(11)
S(23)Au(2)C(15)S(24)	174.7(4)	S(23)C(15)N(3)C(21)	−174.2(6)
S(21)C(8)N(2)C(9)	−1.7(11)	S(24)C(15)N(3)C(16)	−177.3(6)
S(21)C(8)N(2)C(14)	178.6(6)	S(24)C(15)N(3)C(21)	6.6(10)
Cation *C*			
Au(3)S(31)S(32)C(22)	−174.8(6)	S(31)C(22)N(4)C(28)	176.8(8)
S(31)Au(3)C(22)S(32)	−175.2(6)	S(32)C(22)N(4)C(23)	−178.7(8)
S(31)C(22)N(4)C(23)	0.2(15)	S(32)C(22)N(4)C(28)	−2.1(15)
Anion			
Bond	*d*, Å	Bond	*d*, Å
Ag(1)−Cl(1)	2.643(2)	Ag(3)−Cl(2)	2.597(3)
Ag(1)−Cl(1)[c]	2.731(2)	Ag(3)−Cl(4)	2.661(4)
Ag(1)−Cl(2)	2.457(2)	Ag(3)−Cl(5)	2.426(4)
Ag(1)−Cl(3)[c]	2.633(3)	Ag(3)···S(23)	3.304(3)
Ag(2)−Cl(1)	2.614(3)	Ag(1)···Ag(2)	3.4064(15)
Ag(2)−Cl(3)	2.522(3)	Ag(1)···Ag(2)[c]	3.1158(13)
Ag(2)−Cl(4)	2.406(4)		
Angle	ω, deg	Angle	ω, deg
Cl(1)Ag(1)Cl(2)	125.04(9)	Cl(2)Ag(3)Cl(5)	138.99(12)
Cl(1)Ag(1)Cl(1)[c]	90.39(7)	Cl(4)Ag(3)Cl(5)	105.67(13)
Cl(1)Ag(1)Cl(3)[c]	98.48(8)	Ag(1)Cl(1)Ag(1)[c]	89.61(7)
Cl(2)Ag(1)Cl(1)[c]	114.70(9)	Ag(1)Cl(1)Ag(2)	80.77(7)
Cl(2)Ag(1)Cl(3)[c]	121.13(8)	Ag(1)Cl(2)Ag(3)	120.47(10)
Cl(1)Ag(2)Cl(3)	107.22(8)	Ag(2)Cl(1)Ag(1)[c]	71.27(6)
Cl(1)Ag(2)Cl(4)	117.25(11)	Ag(2)Cl(3)Ag(1)[c]	74.34(7)
Cl(3)Ag(2)Cl(4)	129.69(11)	Ag(2)Cl(4)Ag(3)	102.61(13)
Cl(2)Ag(3)Cl(4)	109.55(11)		

* Symmetry transforms: [a] $2-x, 1-y, 1-z$; [b] $1-x, 2-y, 1-z$; [c] $2-x, 1-y, -z$.

vibrations in the −C(S)S− structural fragment: $\nu_{as}(CS_2)$ 1092 cm^{-1} and $\nu_s(CS_2)$ 976 cm^{-1}.

In turn, the absorption bands at 2848 and 2916 cm^{-1} are attributed to stretching vibrations (ν_s and ν_{as}, respectively) of the methylene groups in the seven-membered heterocycles $-N(CH_2)_6$. The weakly intense band at 1467 cm^{-1} corresponds to bending vibrations δ_s of the $-CH_2-$ groups, and the absorption band at 1164 cm^{-1} is due to stretching vibrations of the $N-CH_2$ bonds. Finally, the band at 994 cm^{-1} was attributed to stretching vibrations of the C−C bonds in the cyclic fragments of the HmDtc ligands [24, 25].

The structural organization of complex **I** was determined by direct single-crystal XRD analysis. The

Table 3. Geometric characteristics of hydrogen and chalcogen bonds and anagostic interactions C–H···Ag in complex **I***

Contact D–X···A	Distance, Å			Angle DXA, deg
	D–X	X···A	D···A	
C(2)–H(2*A*)···Cl(5)	0.97	2.79	3.362(12)	118
C(2)^{b}–H(2*B*)^{b}···Cl(5)	0.97	2.94	3.861(10)	158
C(7)^{e}–H(7*B*)^{e}···Cl(3)	0.97	2.93	3.676(11)	135
C(9)^{b}–H(9*B*)^{b}···Cl(4)	0.97	2.83	3.573(13)	134
C(10)^{b}–H(10*A*)^{b}···Cl(3)	0.97	2.92	3.844(11)	159
C(14)^{e}–H(14*B*)^{e}···Cl(1)	0.97	2.92	3.455(10)	116
C(16)–H(16*B*)···Cl(1)	0.97	2.77	3.715(9)	164
C(23)^{b}–H(23*A*)^{b}···Cl(2)	0.97	2.82	3.768(13)	166
C(14)^{e}–H(14*B*)^{e}···Ag(2)	0.97	2.83	3.790(7)	169.6(5)
C(16)–H(16*A*)···Ag(3)	0.97	2.71	3.556(9)	146.5(5)
C(23)^{b}–H(23*A*)^{b}···Ag(3)	0.97	2.70	3.424(11)	131.6(7)
C(1)–S(11)···Cl(2)	1.715(8)	3.392(3)	5.108(8)	179.1(3)
C(1)^{a}–S(12)^{a}···Cl(2)	1.756(8)	3.315(4)	5.069(10)	178.9(3)
C(8)^{b}–S(21)^{b}···Cl(5)	1.733(7)	3.193(6)	4.922(12)	174.6(3)
C(15)^{b}–S(23)^{b}···Cl(5)	1.721(8)	3.443(4)	5.159(8)	175.5(3)

* Symmetry transforms: ^{a} $2-x, 1-y, 1-z$; ^{b} $1-x, 1-y, 1-z$; ^{e} $x, y, -1+z$.

$[Au\{S_2CN(CH_2)_6\}_2]^+$ complex cations and a polynuclear $[Ag_5Cl_9]^{4-}$ anion ares structural units of the studied compound (Fig. 2). The charge of the silver(I) anion predetermines the presence of four gold(III) cations in the structure among which are structurally nonequivalent centrosymmetric cations *A* with the Au(1) atoms, cations *C* with Au(3), and noncentrosymmetric cations *B* with Au(2) in the $A : 2B : C$ ratio (Figs. 3a–3c). When analyzing structural distinctions between the discussed gold(III) cations, it is worth mentioning that in cations *A* and *C* the seven-membered cyclic fragments $-N(CH_2)_6$ of two HmDtc ligands are localized at different sides of the mean plane of the central $[AuS_4]$ fragment (*trans* conformation; Figs. 3a, 3c), whereas in cation *B* they are arranged at one side from the plane (*cis* conformation; Fig. 3b).

The series of common structural features is characteristics of the HmDtc ligands:

– the arrangement of atoms in the C_2NCS_2 groups is close to coplanar, and the highest deviation from the plane is demonstrated by the C(2) and C(21) atoms in

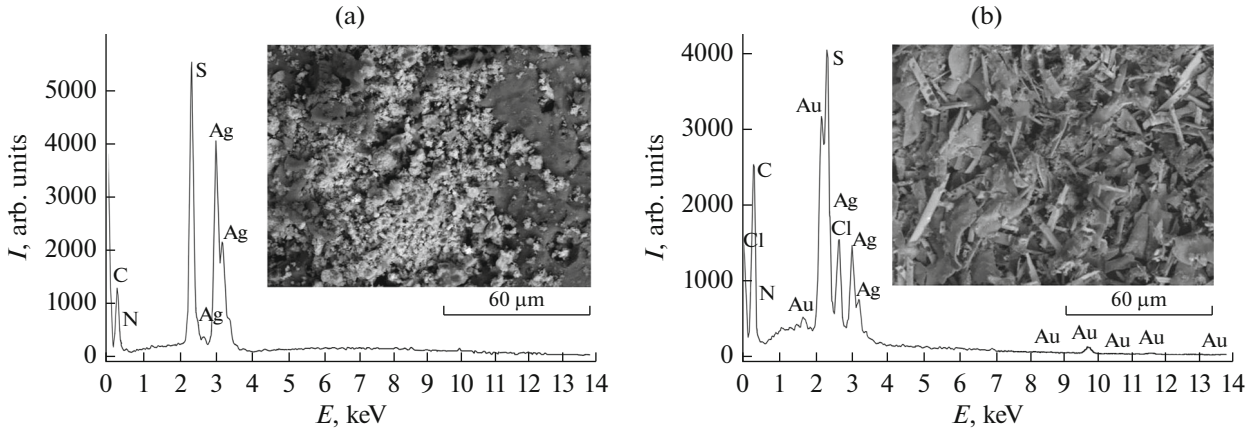

Fig. 1. Particle size and shape and the energy dispersive spectra of the (a) $[Ag(S_2CNHm)]$ and (b) $[Au(S_2CNHm)_2]_4[Ag_5Cl_9]$ complexes.

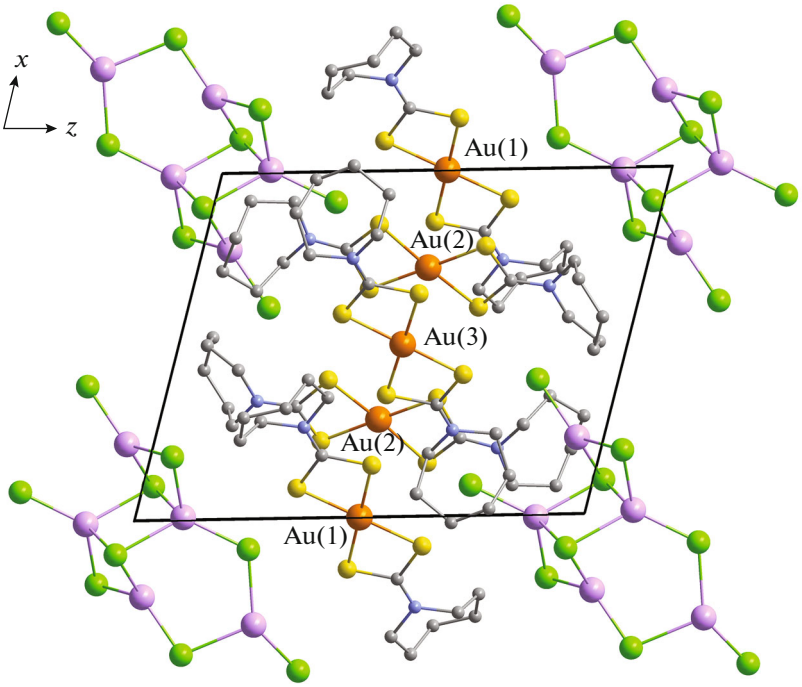

Fig. 2. Packing of structural units in the crystal of complex **I** (projection on the *xz* plane). Hydrogen atoms of the $-CH_2-$ groups are omitted for clarity. Alternative positions of the Ag(3) and Cl(5) atoms in the $[Ag_5Cl_9]^{4-}$ anions are omitted.

cations *A* and *B* (for values of the torsion CNCS angles, see Table 2);

– as expected from the IR spectroscopy data, the formally ordinary N–C(S)S bonds (1.280–1.316 Å) are characterized by an appreciable contribution of double bonding (for comparison, the N–CH_2 bond length lies in a range of 1.451–1.488 Å);

– seven-membered heterocycles $-N(CH_2)_6$ adopt the "twisted chair" conformation [26–28].

An almost *S*,*S*'-isobidentate coordination of the dithiocarbamate ligands (the difference in the Au–S bond lengths does not exceed 0.5%) is accompanied by the formation of four-membered metallocycles [AuS_2C], and in each of the cations the common gold atom combines them into a bicyclic [CS_2AuS_2C] system. The unusually short interatomic distances Au–C (2.813–2.843 Å; for comparison, the sum of the van der Waals radii of these atoms is 3.36 Å [29, 30]) assume the *trans*-annular interaction between the gold and carbon atoms in the discussed metallocycles. It should be noted that the values of the AuSSC and SAuCS torsion angles (Table 2) indicate the coplanar arrangement of the atoms in the cyclic [AuS_2C] groups of cation *A*, whereas in cations *B* and *C* the corresponding angles somewhat differ from 180°: by 5.9° and 5.3° (*B*) and 5.2° and 4.8° (*C*). In all complex gold(III) cations, the [AuS_4] polygons are characterized by the planar tetragonal geometry (or are close to that), which indicates the low-spin dsp^2-hybrid state of the cental gold atom. The S–Au–S diagonal angles in cations *A* and *C* are 180°, whereas in cations *B* they somewhat deviate from 180°: 175.96(8)° and 178.47(8)° due to a minor tetrahedral distortion of the gold(III) polygon.

For cations *A*, *B*, and *C*, the complicated nonachloropentaargentate(I) ion $[Ag_5Cl_9]^{4-}$ (Fig. 3d, Table 2) is the single counterion. Its central moiety contains two four-membered metallocycles [Ag_2Cl_2] comprising the Ag(1)$^{/c}$ and Ag(2)$^{c/}$ silver atoms, which are combined due to pairs of the bridging chlorine atoms Cl(1)$^{c/}$ and Cl(3)$^{c/}$. The Ag–Ag interatomic distance (3.1158(13) Å) in the cycles is essentially less than the sum of the van der Waals radii of two silver atoms (3.44 Å [30]), which indicates the manifestation of the argentophilic ligand-supported interaction [31]. This conclusion is also confirmed by the rhombic geometry of the [Ag_2Cl_2] cycles for which the distance between the oppositely lying silver atoms is by 1.0186 Å shorter than the distance between the chlorine atoms. The ClAgCl angles at the silver atoms are obtuse: 100.83(8)° and 107.22(9)°, whereas those at the chlorine atoms (AgClAg) are acute: 71.27(7)° and 74.36(8)°.

The mentioned structural features are also characteristic of the previously described cyclic anions $[Ag_2Cl_4]^{2-}$ [32–35], although in the $[Ag_5Cl_9]^{4-}$ anion

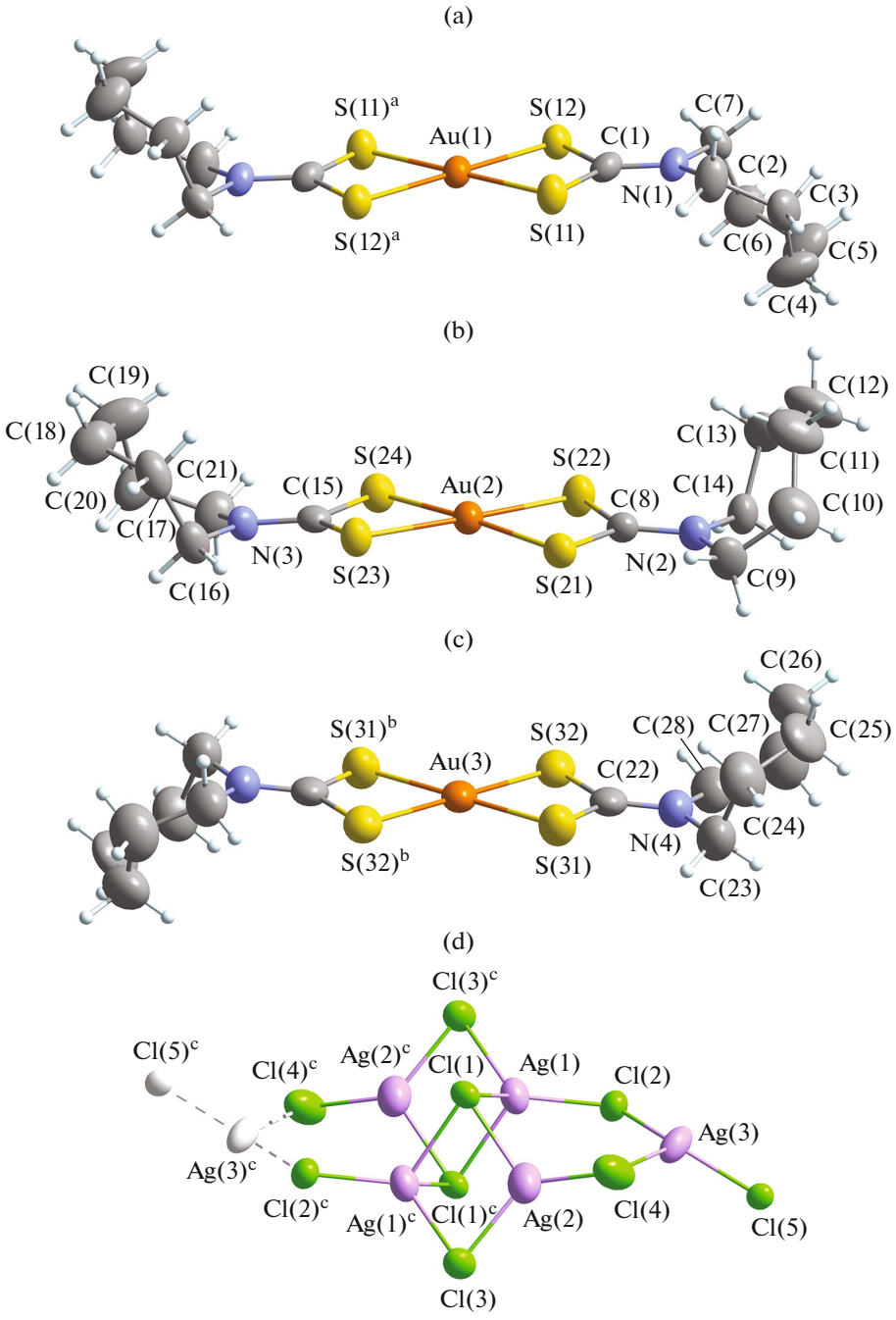

Fig. 3. Structures of three nonequivalent complex cations (a–c) $[Au(S_2CNHm)_2]^+$ and (d) the pentanuclear anion $[Ag_5Cl_9]^{4-}$ (ellipsoids of 50% probability). Uncolored ellipsoids show alternative positions of the Ag(3) and Cl(5) atoms. Symmetry transforms: [a] $2-x, 1-y, 1-z$; [b] $1-x, 2-y, 1-z$; [c] $2-x, 1-y, -z$.

the direct argentophilic interaction is more pronounced. This does not exhaust the structural similarity between the discussed silver(I) anions, since the set of intracyclic Ag–Cl bonds is characterized, in both cases, by an noticeably lower strength than that of the bonds formed outside the cycles.

In the structure of $[Ag_5Cl_9]^{4-}$, the cyclic $[Ag_2Cl_2]$ fragments are linked to each other by the pair symmetric Ag(1)–Cl(1) and Ag(1)^c–Cl(1)^c bonds (2.643(2) Å). Thus, the Cl(1) and Cl(1)^c atoms perform the μ_3-structural function determining a fourfold, distorted tetrahedral, environment $[Cl_4]_2$ for the Ag(1) and Ag(1)^c atoms, which have sp^3-hybrid state.

[2] The methodical approaches [36], which made it possible to determine the 81% contribution of the tetrahedral component to the geometry of the $[AgCl_4]$ polyhedra were used for the quantitative characterization of the Ag(1) and Ag(1)^c polyhedra.

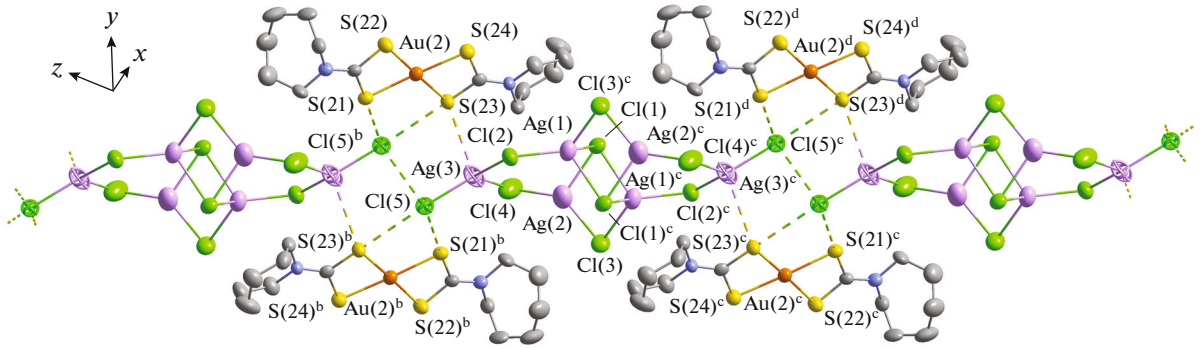

Fig. 4. Fragment of the supramolecular ribbon in the structure of compound **I** formed due to the secondary interactions Ag···S, Cl···S, and Cl···Cl between the silver(I) anions and isomeric Au^{3+} cations *B* (shown by dash). Symmetry transforms: [b] $1-x, 1-y, 1-z$; [c] $2-x, 1-y, -z$; [d] $1+x, y, -1+z$.

In turn, the μ_2-Cl(2) and μ_2-Cl(4) bridging atoms combiine the central moiety of the anion with the peripheral silver atom Ag(3) (Fig. 3d). Note that the Ag(3) and Cl(5) atoms are randomly distributed between two structural positions with the same population 0.5. The Ag(2) and Ag(3) atoms form a trifold environment [Cl_3] (sp^2-hybrid state). Nevertheless, the geometry of the distorted [$AgCl_3$] polygons deviates from the planar geometry due to some shift of the central silver atom from the plane formed by the chlorine atoms: the sum of the internal ClAgCl angles is noticeably less than 360° (354.16° and 354.22°, respectively).

The subsequent self-organization of the ionic structural units in compound **I** into a complicated supramolecular structure occurs due to the cation-anionic nonvalent interactions Cl···S and Ag···S. Being a binding node, each complex anion $[Ag_5Cl_9]^{4-}$ forms nonsymmetric secondary bonds[3] Cl···S with the sulfur atoms in the inner sphere of noncentrosymmetric gold cations *B* due to the statistically distributed terminal chlorine atoms Cl(5): Cl(5)···S(21) 3.193(6) Å and Cl(5)···S(23) 3.443(4) Å (Fig. 4); for comparison, the sum of the van der Waals radii of the chlorine and sulfur atoms is 3.55 Å [29]. (According to published data [38, 39], the discussed secondary interactions (Table 3) should be classified as chalcogen bonds.) In addition, the disordered Ag(3) atoms form secondary bonds with the S(23) atoms of another pair of cations *B*: Ag(3)···S(23) 3.304(3) Å. This results in the building up of the metal polyhedron to the elongated trigonal pyramid [$AgCl_3S$] (Fig. 4); the sum of the van der Waals radii of the silver and sulfur atoms is 3.52 Å [29, 30]. In addition, the interaction between the terminal Cl(5) atoms of the nearest silver(I) anions induces the formation of the interhalogen secondary bond Cl(5)···Cl(5)[b] (3.198(7) Å) [13, 40–42] (for comparison, the sum of the van der Waals radii of two chlorine atoms is 3.50 Å [29]), which also contributes to the overall stabilization of supramolecular structure **I**. All of the discussed secondary interactions (Cl···S, Ag···S, and Cl···Cl) results in the formation of the supramolecular ribbon $\{\cdots[Ag_5Cl_9]^{4-}\cdots 2B^+\}_n$, which includes the alternating polynuclear silver(I) anions and pairs of noncentrosymmetric gold(III) cations *B* (Fig. 4).

The structural function of isomeric centrosymmetric cations *A* is to combine the supramolecular ribbons into the 2D pseudo-polymer network (Fig. 5). Therefore, each of the discussed cations, localized in the volume between the ribbons, is a double linker having two pairs of nonsymmetric secondary bonds with the chlorine atoms of the $[Ag_5Cl_9]^{4-}$ anions, which are part of neighboring supramolecular formations: Cl(2)···S(11) 3.392(3) Å and Cl(2)···S(12) 3.315(4) Å (Fig. 5, Table 3). In turn, isomeric cations *C* localized between the 2D pseudo-polymer layers participate in their symmetric binding to form the 3D supramolecular architecture (Fig. 6). The symmetric C(23)[b]–H(23*A*)[b]···Cl(2) hydrogen bonds (distances H···Cl 2.82 Å and C···Cl 3.768 Å, angle C–H···Cl 166°) and anagostic interactions C(23)[b]–H(23*A*)[b]···Ag(3) (distance H···Ag 2.70 Å, angle C–H···Ag 131.6°) (Fig. 6, Table 3) are the most significant interionic interactions of each cation *C*. The latter fall on the corresponding ranges (2.3–2.9 Å and 110°–170°) that characterize secondary interactions of this type [43]. It should be noted that cation *B* is also involved in the anagostic interactions C(16)–H(16*A*)···Ag(3) and C(14)[e]–H(14*B*)[e]···Ag(2): the H···Ag distances are 2.71 and 2.83 Å, and the C–H···Ag angles are 146.5° and 169.6°, respectively. In addition, all silver atoms of the $[Ag_5Cl_9]^{4-}$ anion and $-CH_2-$ group of the cyclic fragments of the ligands interact via the system of the C–H···Cl bonds (Table 3).

[3] The concept of secondary bonds was proposed for the description of nonvalent type interactions between atoms at the distances comparable with the sum of their van der Waals radii [37].

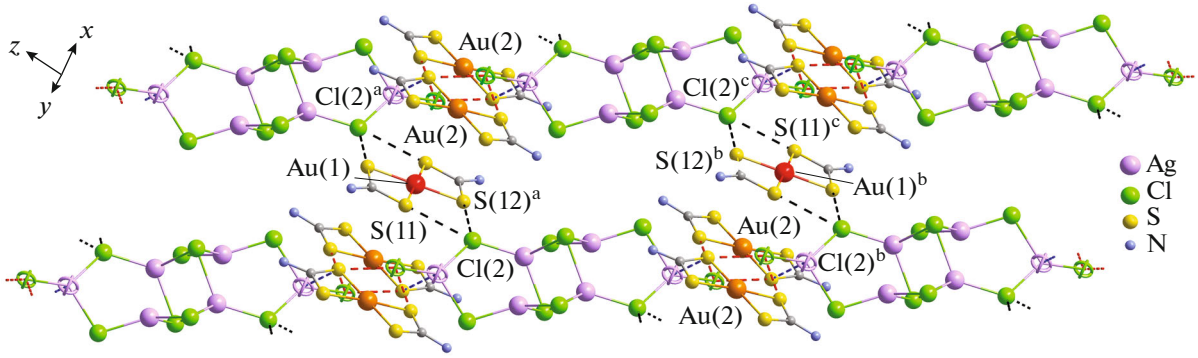

Fig. 5. Fragment of the 2D coordination network: joining of the supramolecular ribbons by isomeric cations *A* due to the pair secondary interactions Cl···S (shown by dash). Symmetry transforms: [a] 2 – *x*, 1 – *y*, 1 – *z*; [b] 1 + *x*, *y*, –1 + *z*; [c] 3 – *x*, 1 – *y*, –*z*.

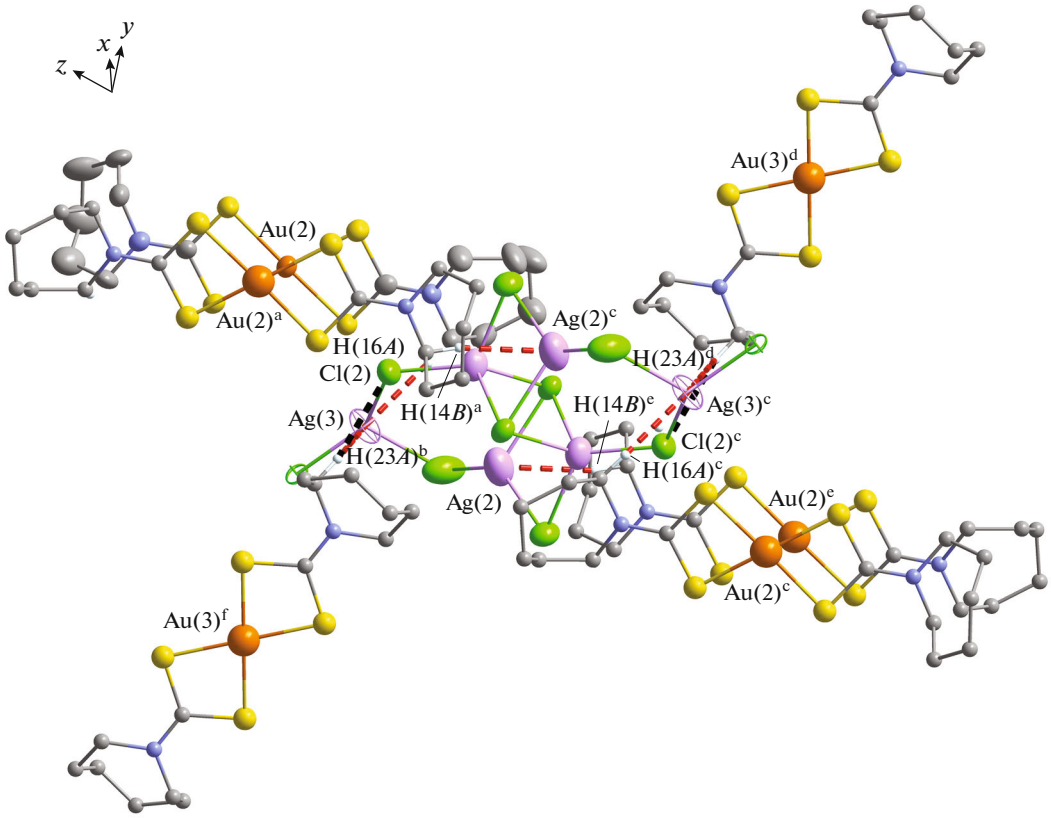

Fig. 6. Steric orientation of isomeric gold cations *C* for binding the adjacent pseudo-polymer layers into the 3D framework. Anagostic interactions C–H···Ag and hydrogen bonds C–H···Cl between the silver(I) anions and gold(III) cations *C* and *B* (shown by dash). Symmetry transforms: [a] 2 – *x*, 1 – *y*, 1 – *z*; [b] 1 – *x*, 1 – *y*, 1 – *z*; [c] 2 – *x*, 1 – *y*, –*z*; [d] 1 + *x*, *y*, –1 + *z*; [e] *x*, *y*, –1 + *z*; [f] *x*, –1 + *y*, *z*.

The thermal behavior of compound **I** was studied by STA in an argon atmosphere using parallel detection of the TG and DSC curves (Fig. 7). The studied compound is thermally stable to ~140°C. The main mass loss is detected on the TG curve in a temperature range of ~140–403°C (Fig. 7*a*). The discussed part of the TG curve contains two inflection points (at 235 and 294°C), which divide the curve into three sections indicating a complicated character of the thermal transformations of substance **I**. Nevertheless, an overall loss of 49.72% (of the initial mass of the complex) in the discussed temperature range directly indicates the reduction of gold to the elemental state and the liberation of AgCl (calculated 50.52%). The final flat region of the TG curve (~403–800°C) is due to the continuing desorption of volatile thermolysis products and the subsequent reduction of silver (from AgCl) to the elemental state. At the end of thermolysis at

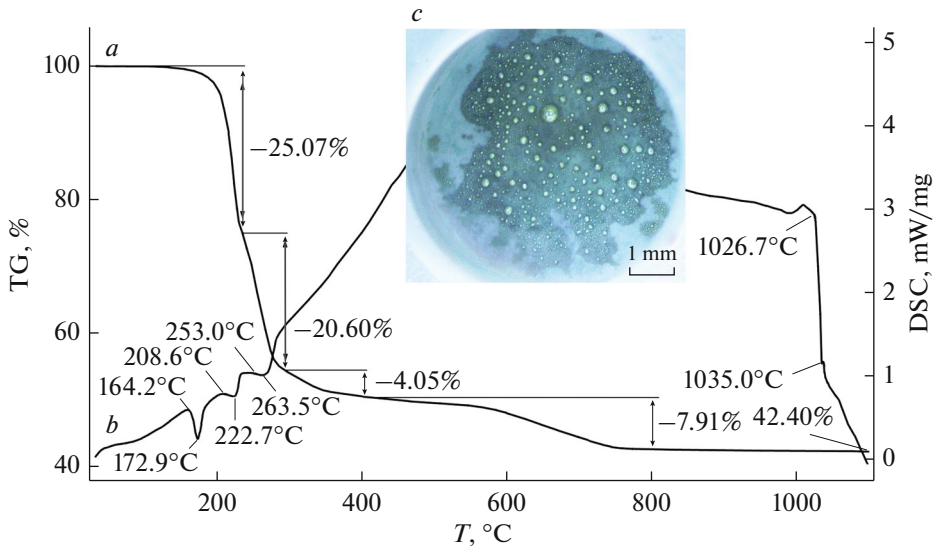

Fig. 7. (*a*) TG and (*b*) DSC curves of complex **I** and (*c*) the photograph of the crucible bottom after the end of thermolysis.

1100°C, light yellow round metallic particles of a gold–silver alloy were found on the crucible bottom (Fig. 7*c*), whose mass (42.40%) is somewhat lower than the overall calculated value (43.65%) for the reduced metals.

The DSC curve of complex **I** reflects a series of thermal effects (Fig. 7*b*). The first endoeffect with an extreme at 172.9°C is due to sample melting: the extrapolated m.p. is 164.2°C. (As found by the independent determination in a glass capillary, the melting of complex **I** was established to occur in a range of 170–172°C.) The subsequent endoeffects with extremes at 222.7 and 263.5°C are related to the intense thermolysis stages of complex **I**, since they are projected onto two regions of the main mass loss on the TG curve. Finally, the endoeffect indicating the melting of the metals reduced to the elemental state (the extrapolated m.p. is 1026.7°C) was observed in the high-temperature range of the DSC curve.

Complex **I** and, hence, the gold–silver alloy derived from it are characterized by the atomic ratio Au : Ag = 4 : 5 (1 : 1.25). Beside that, we previously obtained a series of the double complexes of $[Au(S_2CNR_2)_2][AgCl_2]$ (R = Et [16], Pr [17], ^{i}Bu [15]) and $[Au\{S_2CN(CH_2)_5\}_2]_2[Ag_2Cl_4]\cdot CH_2Cl_2$ [44], whose ratio Au : Ag = 1 : 1. A comparison of the extrapolated m.p. values of the Au–Ag alloys formed by the thermolysis of the aforementioned complexes (1031.8°C [16], 1030.4°C [17], 1029.7°C [15], 1033.4°C [44]) and compound **I** shows the least value in the last case (1026.7°C), which objectively indicates a higher silver content in this alloy. An analysis of the phase diagram of the Au–Ag binary metallic system [45] suggests more certainly that m.p. = 1026.7°C corresponds to the atomic ratio of the components (Au : Ag) in the prepared alloy, which is close to 1 : 1.25.

CONCLUSIONS

To conclude, a new double Au(III)–Ag(I) pseudopolymer complex $[Au\{S_2CN(CH_2)_6\}_2]_4[Ag_5Cl_9]$ was synthesized in a preparative yield and characterized in detail by the XRD, IR spectroscopy, and STA data. The compound was found to contain three isomeric forms of gold(III) cations $[Au\{S_2CN(CH_2)_6\}_2]^+$ (in the ratio $A : 2B : C$) that perform different structural functions and the pentanuclear silver anion $[Ag_5Cl_9]^{4-}$. The determining role of the multiple interionic secondary bonds Cl···S and Ag···S, hydrogen bonds C–H···Cl, and anagostic interactions C–H···Ag in the formation of the complicated three-dimensional supramolecular architecture of complex **I** was shown. The possibility of the quantitative regeneration of the metals comprising the Au(III)–Ag(I) complex was found by studying the thermal behavior of complex **I**.

ACKNOWLEDGMENTS

Elemental analysis and IR spectroscopy were carried out using the equipment of the Center for Collective Use of Physical Methods of Investigation at the Kurnakov Institute of General and Inorganic Chemistry (Russian Academy of Sciences). Electron microscopy, X-ray spectral studies, and determination of the gold content in solutions were carried out at the Center for Collective Use "Amur Center of Mineralogical and Geochemical Studies" of the Institute of Geology and Nature Management (Far Eastern Branch, Russian Academy of Sciences).

FUNDING

This work was supported by ongoing institutional funding. No additional grants to carry out or direct this particular research were obtained.

CONFLICT OF INTEREST

The authors of this work declare that they have no conflicts of interest.

REFERENCES

1. Janz, D.M., *Dithiocarbamates*, in *Encyclopedia of Toxicology*, P. Wexler, Ed., Elsevier, 2014, vol. 2, 3rd ed., p. 212.
2. Kaul, L., Süss, R., Zannettino, A., and Richter, K., *iScience*, 2021, vol. 24, no. 2, p. 102092.
3. Sauna, Z.E., Shukla, S., and Ambudkar, S.V., *Mol. BioSyst.*, 2005, vol. 1, no. 2, p. 127.
4. Skrott, Z., Mistrik, M., Andersen, K.K., et al., *Nature*, 2017, vol. 552, p. 194.
5. Li, H., Wang, J., Wu, C., et al., *Drug Discov. Today*, 2020, vol. 25, no. 6, p. 1099.
6. McMahon, A., Chen, W., and Li, F., *J. Control. Release*, 2020, vol. 319, p. 352.
7. Hogarth, G., *Mini-Rev. Med. Chem.*, 2012, vol. 12, no. 12, p. 1202.
8. Williams, M.R.M., Bertrand, B., Hughes, D.L., et al., *Metallomics*, 2018, vol. 10, no. 12, p. 1655.
9. Le, H.V., Babak, M.V., Ehsan, M.A., et al., *Dalton Trans.*, 2020, vol. 49, no. 22, p. 7355.
10. Adokoh, C.K., *RSC Adv.*, 2020, vol. 10, no. 5, p. 2975.
11. Oladipo, D., Mocktar, C., and Omondi, B., *Arabian J. Chem.*, 2020, vol. 13, no. 8, p. 6379.
12. Abás, E., Aguirre-Ramírez, D., Laguna, M., and Grasa, L., *Biomedicines*, 2021, vol. 9, no. 12, p. 1775.
13. Oladipo, D., Tolufashe, G.F., Mocktar, C., and Omondi, B., *Inorg. Chim. Acta*, 2021, vol. 520, 120316.
14. Loseva, O.V., Lutsenko, I.A., Rodina, T.A., et al., *Polyhedron*, 2022, vol. 226, p. 116097.
15. Korneeva, E.V., Smolentsev, A.I., Antzutkin, O.N., and Ivanov, A.V., *Inorg. Chim. Acta*, 2021, vol. 525, 120383.
16. Korneeva, E.V., Loseva, O.V., Smolentsev, A.I., and Ivanov, A.V., *Russ. J. Gen. Chem.*, 2018, vol. 88, no. 8, p. 1680. https://doi.org/10.1134/S1070363218080200
17. Korneeva, E.V., Smolentsev, A.I., Antzutkin, O.N., and Ivanov, A.V., *Russ. Chem. Bull., Int. Ed.*, 2019, vol. 68, no. 1, p. 40. https://doi.org/10.1007/s11172-019-2413-7
18. Korneeva, E.V., Novikova, E.V., Loseva, O.V., et al., *Russ. J. Coord. Chem.*, 2021, vol. 47, no. 11, p. 769. https://doi.org/10.1134/S1070328421090050
19. Byr'ko, V.M., *Ditiokarbamaty* (Dithiocarbamates), Moscow: Nauka, 1984.
20. Korneeva, E.V., Ivanov, A.V., Gerasimenko, A.V., et al., *Russ. J. Gen. Chem.*, 2019, vol. 89, no. 8, p. 1642. https://doi.org/10.1134/S1070363219080152
21. Loseva, O.V., Rodina, T.A., Ivanov, A.V., et al., *Russ. J. Coord. Chem.*, 2018, vol. 44, no. 10, p. 604. https://doi.org/10.1134/S107032841810007X
22. *APEX2 (version 1.08), SAINT (version 7.03), SADABS (version 2.11)*, Madison: Bruker AXS Inc., 2004.
23. Sheldrick, G.M., *Acta Crystallogr., Sect. C.: Struct. Chem.*, 2015, vol. 71, no. 1, p. 3.
24. Kazitsyna, L.A. and Kupletskaya, N.B., *Primenenie UF-, IK-, YaMR- i mass-spektroskopii v organicheskoi khimii* (Applications of UV, IR, NMR, and Mass Spectroscopy in Organic Chemistry), Moscow: Mosk. Univ., 1979.
25. Gremlikh, G.U., *Yazyk spektrov. Vvedenie v interpretatsiyu spektrov organicheskikh soedinenii* (Language of Spectra. Introduction to Interpretation of the Spectra of Organic Compounds), Moscow: LLC Bruker Optik, 2002.
26. Bocian, D.F., Pickett, H.M., Rounds, T.C., and Strauss, H.L., *J. Am. Chem. Soc.*, 1975, vol. 97, no. 4, p. 687.
27. Boessenkool, I.K. and Boeyens, J.C.A., *J. Cryst. Mol. Struct.*, 1980, vol. 10, nos. 1–2, p. 11.
28. Entrena, A., Campos, J., Gómez, J.A., et al., *J. Org. Chem.*, 1997, vol. 62, no. 2, p. 337.
29. Bondi, A., *J. Phys. Chem.*, 1964, vol. 68, no. 3, p. 441.
30. Bondi, A., *J. Phys. Chem.*, 1966, vol. 70, no. 9, p. 3006.
31. Schmidbaur, H. and Schier, A., *Angew. Chem., Int. Ed. Engl.*, 2015, vol. 54, no. 3, p. 746.
32. Helgesson, G. and Jagner, S., *Dalton Trans.*, 1988, no. 8, p. 2117.
33. Helgesson, G. and Jagner, S., *Dalton Trans.*, 1990, no. 8, p. 2413.
34. Hassan, A., Breeze, S.R., Courtenay, S., et al., *Organometallics*, 1996, vol. 15, no. 26, p. 5613.
35. Aboulkacem, S., Tyrra, W., and Pantenburg, I., *J. Chem. Cryst.*, 2006, vol. 36, no. 2, p. 141.
36. Yang, L., Powel, D.R., and Houser, R.P., *Dalton Trans.*, 2007, no. 9, p. 955.
37. Alcock, N.W., *Adv. Inorg. Chem. Radiochem.*, 1972, vol. 15, no. 1, p. 1.
38. Wang, W., Ji, B., and Zhang, Y., *J. Phys. Chem. A*, 2009, vol. 113, no. 28, p. 8132.
39. Scilabra, P., Terraneo, G., and Resnati, G., *Acc. Chem. Res.*, 2019, vol. 52, no. 5, p. 1313.
40. Reddy, C.M., Kirchner, M.T., Gundakaram, R.C., et al., *Chem. Eur. J.*, 2006, vol. 12, no. 8, p. 2222.
41. Awwadi, F.F., Willett, R.D., Peterson, K.A., and Twamley, B., *Chem. Eur. J.*, 2006, vol. 12, no. 35, p. 8952.
42. Usoltsev, A.N., Korobeynikov, N.A., Novikov, A.S., et al., *Inorg. Chim. Acta*, 2020, vol. 513, p. 119932.
43. Rajput, G., Singh, V., Gupta, A.N., et al., *CrystEngComm*, 2013, vol. 15, no. 23, p. 4676.
44. Korneeva, E.V., Lutsenko, I.A., Bekker, O.B., et al., *Russ. J. Coord. Chem.*, 2022, vol. 48, no. 12, p. 924. https://doi.org/10.1134/S1070328422700063
45. *Diagrammy sostoyaniya dvoinykh metallicheskikh sistem: spravochnik* (Phase Diagrams of Binary Metallic Systems), Lyakishev, N.P., Ed., Moscow: Mashinostroenie, 1996.

Translated by E. Yablonskaya